

An in-situ SERS Study of the Interfacial Behaviour of Coumarin During the Electrodeposition of Cobalt

Benedetto Bozzini and Lucia D'Urzo*

Universita' del Salento, Brindisi Fuel Cell Durability Laboratory, Cittadella della Ricerca, I-72100 Brindisi - Italy

*E-mail: benedetto.bozzini@unile.it

Received: 13 May 2009 / *Accepted:* 20 June 2009 / *Published:* 19 July 2009

In this study we report in situ SERS measurements carried out during electrodeposition and stripping of Co films, using Au electrodic substrates and an acidic sulphate bath containing coumarin. We demonstrated the SERS activity of Co during both cathodic growth and the anodic stripping, under suitable conditions. Potential- and time-dependent adsorption and electrodic reactivity of coumarin were found. Furthermore, the stripping measurements revealed a notable sensitivity of the SERS activity on the coating structure. Density Functional Theory (DFT) calculation of Raman spectra has been used to identify the cathodic reaction and hydrolysis products of coumarin, corresponding to modifications of the SERS spectra.

Keywords: Electrodeposition, SERS, Cobalt, Coumarin, DFT

1. INTRODUCTION

The electrodeposition of Co and its alloys has met extensive industrial interest for many decades, with applications ranging from electrowinning (e.g. [1]) to the fabrication of magnetic devices in the computer industry for both hard disks and memory systems (e.g. [2, 3]). Furthermore, electrodeposited Co structures just larger than the superparamagnetic critical dimensions have received great attention in recent years, because of their possible application in non-volatile magnetic random access memory devices (e.g. [4]). Electrodeposited Co nanostructures have been recently fabricated using alumina templates [5] and soft lithography approaches [6].

Co electrodeposition baths typically contain boric acid to control the pH of the catholyte and different types of organic additives, aimed at the achievement of structures related - in a largely still unknown way - to the sought-after functional properties. Grain refinement is a generally desirable feature of electrodeposited Fe-group metals and coumarin is a typical additive used for this purpose

(e.g. [7, 8]). Notwithstanding the widespread use of this additive, relatively few studies have been carried out on coumarin effects on electrocrystallization [9-13]; in particular, we are not aware of studies related to the adsorption behavior of coumarin during electrodeposition processes.

In this paper we address the problem of clarifying the cathodic action of coumarin with a molecular approach, based on in situ spectroelectrochemistry and DFT modelling. SERS has been chosen as the experimental method of choice because of the possibility of carrying out surface vibrational spectroscopy with a thick layer of aqueous electrolyte and in the presence of hydrogen bubble evolution. Of course, Co is not generally regarded as a SERS-active metal, but it has been proved relatively recently (see e.g. [14, 15] for comprehensive reviews) that the SERS effect - though at a significantly lower level with respect to precious metals - can be achieved also with Fe- and Pt-group metals. To the best of the authors' knowledge, the only reports of SERS work with Co electrodes deal with: (i) the adsorption of pyridine at chemically-electrochemically etched surfaces [16] and (ii) the electrodeposition of nano-wire arrays [17]. The use of SERS in electrodeposition studies of such transition metals has received very limited attention: apart from the previously mentioned nano-wire growth work - also involving Ni, Pt and Pd in addition to Co [17] -, Ni electrodeposition has been used in one case to achieve suitable roughening of a Ni electrode for SERS work [18].

2. EXPERIMENTAL PART

2.1. Experimental

The Co electrodeposition bath was: $\text{CoSO}_4 \cdot 7\text{H}_2\text{O}$ 1M, H_3BO_3 0.7M, pH 2.2. Analytic grade chemicals were dissolved in ultra-pure water of conductivity 18.2 $\text{M}\Omega \text{ cm}$, obtained with a Millipore Milli-Q system. The solutions were deaerated and continuously purged with Ar.

SERS spectra were recorded using a LabRam microprobe confocal system. A 50 \times long-working-distance objective was used, the excitation line at 632.8 nm was provided by a 12 mW He-Ne laser. The slit and pinhole were set at 200 and 400 μm , respectively, corresponding to a scattering volume of ca. 3 pL; Raman spectra were acquired with a 600 grid/mm spectrometer. The recorded Raman intensities are directly proportional to the discharge current of the CCD detector. In situ electrochemical measurements were performed in a Ventacon glass cell equipped with a glassy carbon disc electrode (O 5 mm) embedded in Teflon holders. The electrode was coated with a Au film, 20 nm thick, electrodeposited at 10 mA cm^{-2} from the following solution: $\text{KAu}(\text{CN})_2$ 35 mM, citric acid 0.2M, NH_4^+ -citrate 0.15M, pH 6,4, T 40°C. The counter electrode was a Pt wire loop of total area ca. 2 cm^2 , concentric and coplanar with the Au-plated working electrode. An external Ag/AgCl reference electrode was used and all the potentials were reported on this scale. All the experiments were run at room temperature.

2.2. DFT calculations

The simulation of geometrical and vibrational properties of coumarin and its main reaction products has been carried out with the Gaussian 03 package [19]. According to [13], we modelled

coumarin and the following set of candidate reaction products: (i) ortho-hydrocynamic acid (SH), (ii) 3-2-hydroxy-phenyl-propionic acid (S2); (iii) o- hydroxy-phenyl-propanol (S3); (iv) n-propyl-phenol (S4). The optimised geometry and the Raman vibrational spectra of the above structures have been simulated in the framework of the Density Functional Theory (DFT), with the B3LYP hybrid functional, and basis set 6-311++g(d), the corresponding optimised geometries are shown in Figure 1. In order to correct the systematic overestimation of the calculated Raman shift, a rescaling factor of 0.98 has been applied according to the specific functional and basis sets used [20].

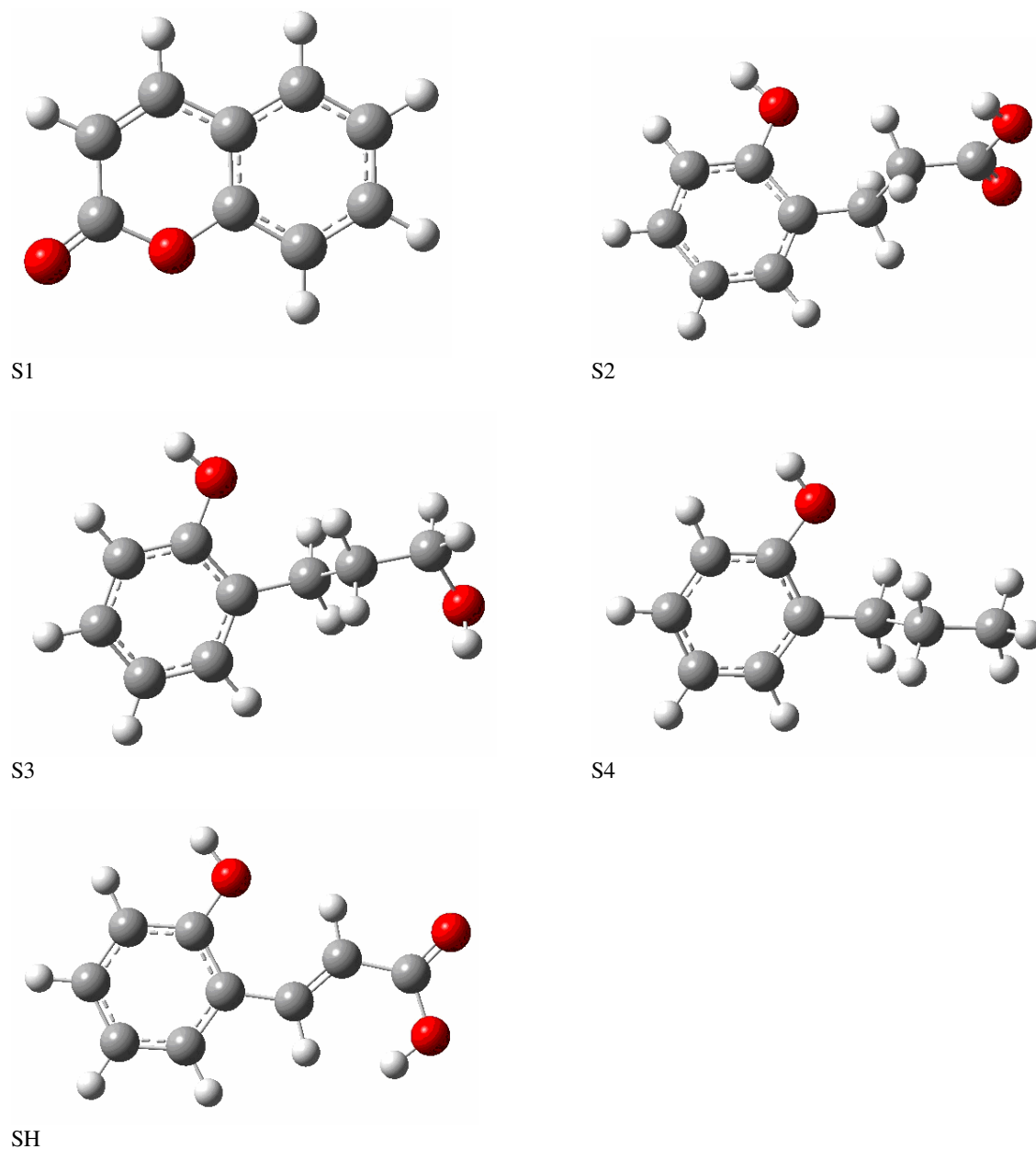


Figure 1. Optimized geometries – computed by DFT- B3LYP/6-31+g(d) - of the following molecules: coumarin (S1), 3-2-hydroxy phenyl propionic acid (S2), o-hydroxy phenyl propanol (S3), n-propyl phenol (S4), o-hydroxy cinnamic acid (SH).

3. RESULTS AND DISCUSSION

In order to study the electrodic behaviour of coumarin in the Co bath, we carried out the following types of Raman measurements: (i) at open-circuit potential (OCP) on both Au and Co surfaces (Section 3.1); (ii) during the application of a cathodic potential staircase (Section 3.2); (iii) during cathodic potentiostatic polarisation (Section 3.3); (iv) during the potentiostatic stripping of electrodeposited Co films (Section 3.4).

Spectral interpretation of electrochemical Raman experiments is based on: (i) Normal-Raman measurements of coumarin powder; (ii) comparison with spectral databanks [21] and other compilations of vibrational spectroscopy data [22]; (iii) DFT computations.

3.1. Raman measurements at open-circuit potential

A first series of SERS experiments was performed at open-circuit potential (OCP) in the Co bath at both Au and Co active surfaces. Under these conditions high-quality spectra could be measured, reported in Figures 2 (Au surface) and 3 (Co surface); we repeated both types of measurements for times in excess of 45 min and we always obtained spectra exhibiting the same pattern and quality. Active Au surfaces were obtained by potentiostatic stripping of pre-electrodeposited Co layers, according to the procedure detailed below in Section 3.4 a stable OCP value of 231 ± 3 mV was recorded. Co layers, SERS active at OCP (-78 ± 5 mV) in the coumarin-containing bath, were prepared as follows: starting from a clean Au surface, we applied a cathodic-anodic potential square-wave - terminated cathodically -, switching from -50 to $+50 \mu\text{A cm}^{-2}$, with a period of 30 s; 6 cycles were enough to obtain a notable surface activation. The SERS-activity is probably obtained through to the SERS-borrowing mechanism pinpointed in [23, 24].

3.2. Electrodeposition of Co with cathodic potential staircase

During this type of experiments, we applied a cathodic potential staircase starting from the OCP of 231 mV and stepping initially to 200 mV and then up to -800 mV in steps of 50 mV lasting 2 min each. A SERS spectrum was recorded during each potentiostatic step. Of course, the spectra recorded in this particular experiment exhibit an intrinsic serial correlation; mutually independent potential-dependent experiments - of both transient and steady-state types - will be described in Section 3.3.

In Figure 4 we report a sequence of spectra taken at the indicated potential values during the cathodic potentiostatic staircase. At potentials less cathodic than -650 mV, weak bands are observed, corresponding to the vibration of the aromatics ring belonging to coumarin-related species (identified with Greek letters without apex, see Table 1 for the mode assignment). These bands are better resolved in spectra measured with longer deposition times, as discussed in Section 3.3. As the cathodic overpotential increases, these bands tend to fade out, possibly owing to the growth of non-enhancing crystallites in this potential range. Apart from the coumarin-related bands, in Figure 4 (in particular in Figure 4A) it is also possible to observe the following features: (i) the intramolecular stretching peak

$\nu(\text{CN})$ of adsorbed CN^- – exhibiting Stark tuning - and (ii) the corresponding extramolecular Au-C stretching band $\nu(\text{Au-C})$. These peaks are due to CN^- incorporated in the Au substrate, as proved in [25]. The intensity of these bands - that decreases with increasing cathodic polarisation -, can be used as a marker of the degree of coverage of the Au electrode with electrodeposited Co (Figure 5).

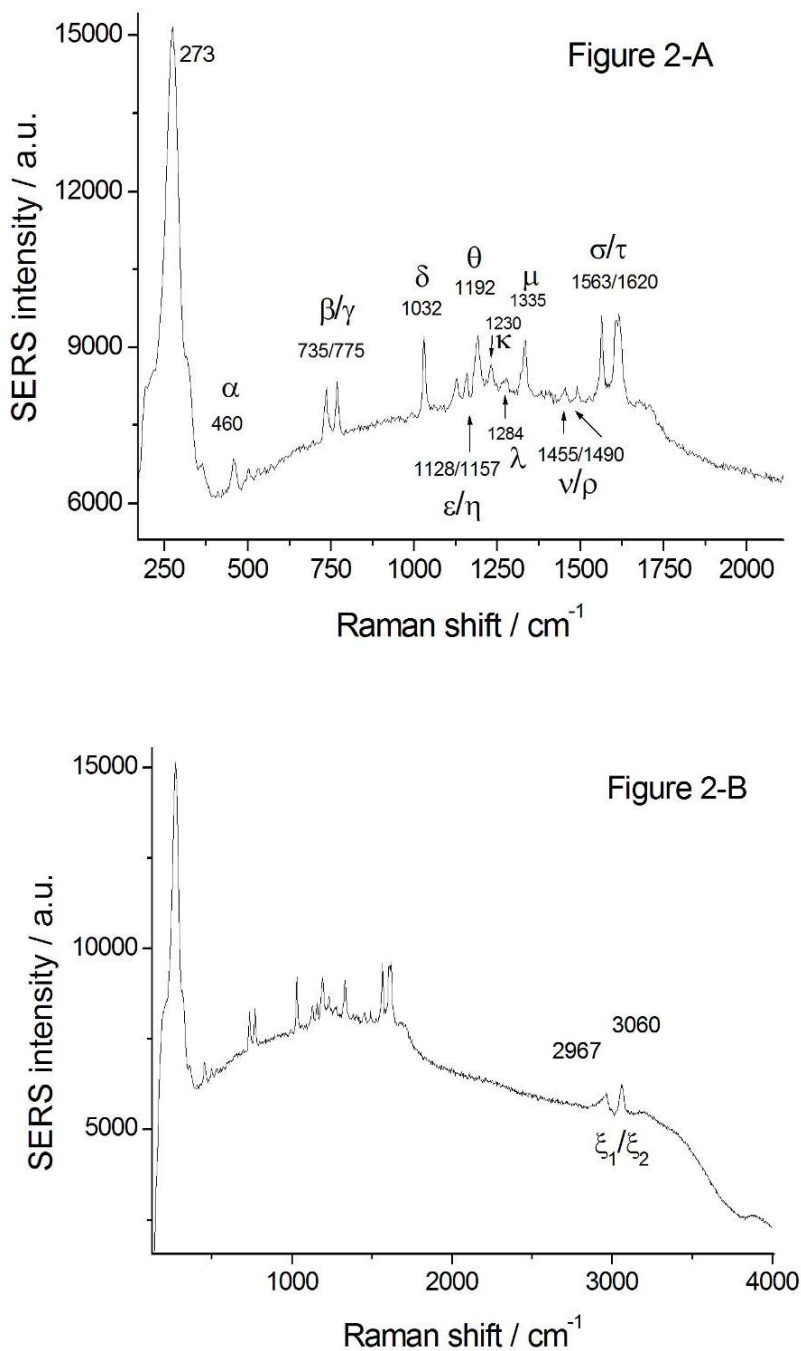


Figure 2. SERS spectrum recorded at open-circuit potential at a Au electrode in contact with the coumarin-containing Co bath.

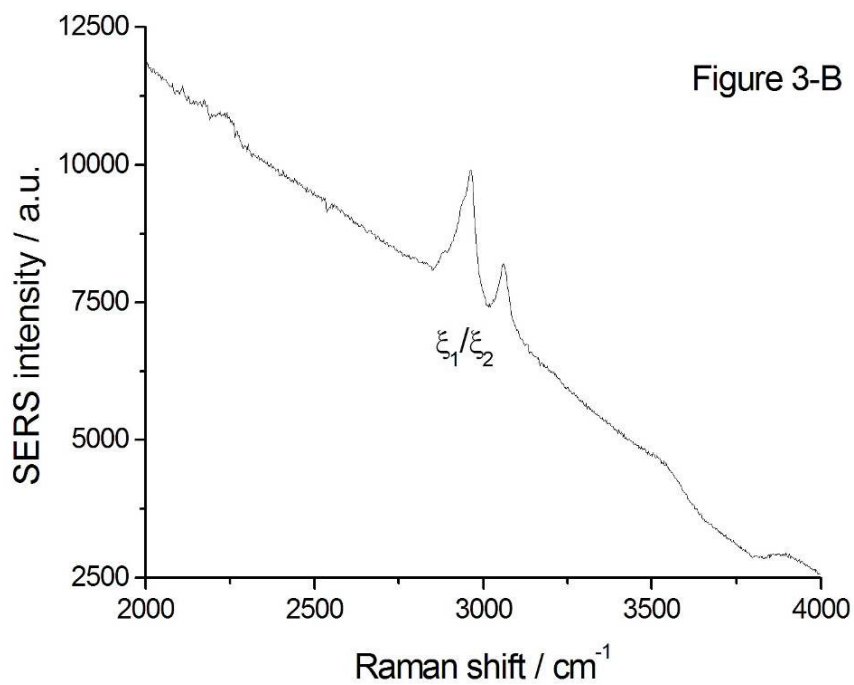
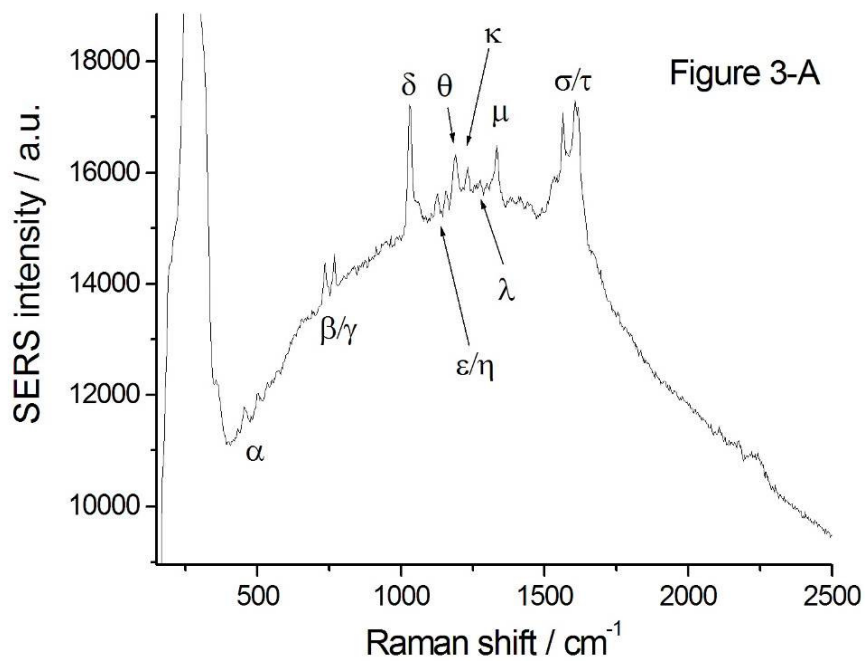


Figure 3. SERS spectrum recorded at open-circuit potential at an electrodeposited Co layer in contact with the coumarin-containing Co bath.

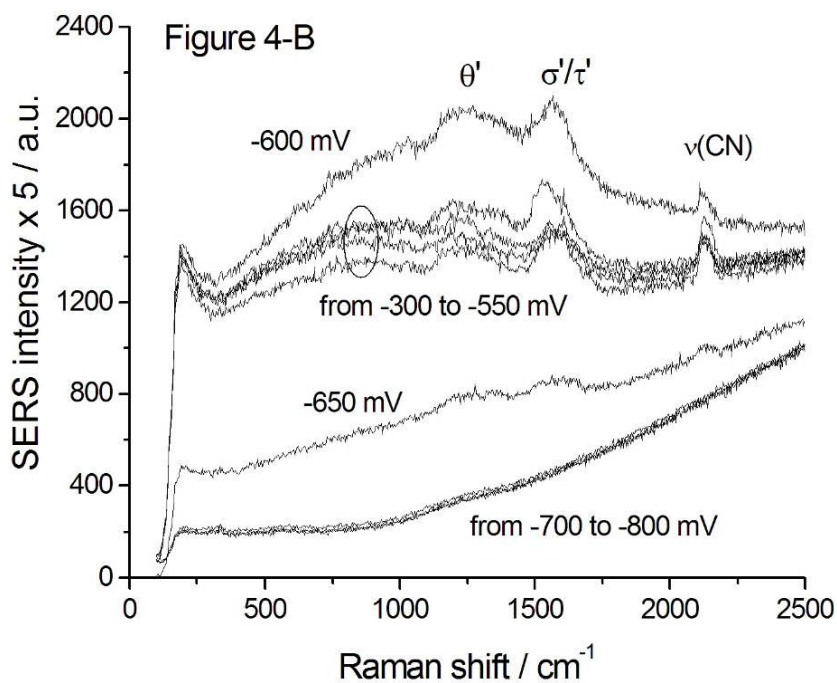
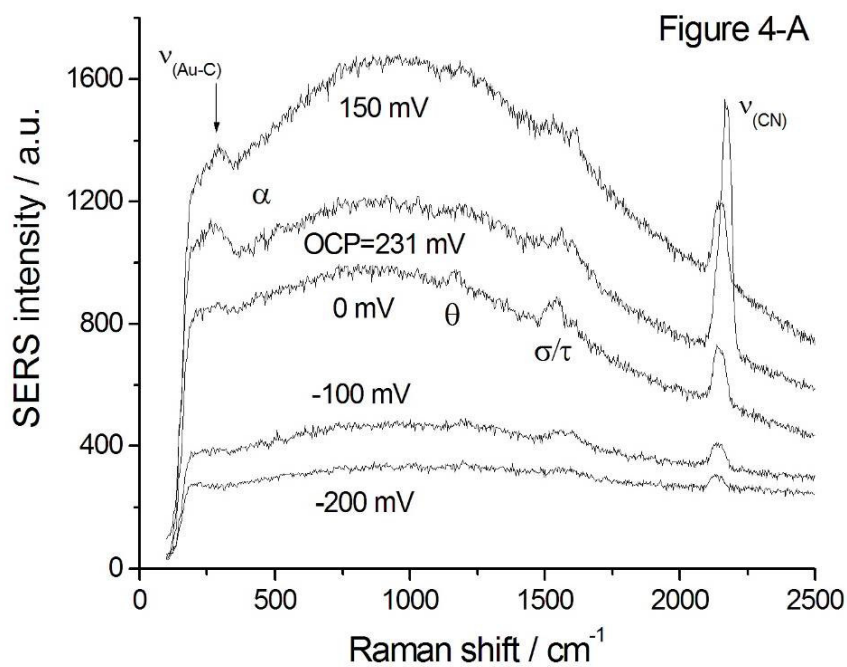


Figure 4. In situ SERS spectra recorded during the electrodeposition of Co from a bath containing coumarin. A cathodic potentiostatic staircase was applied as indicated in the figure. (A) Potential values from OCP to -200 mV (Ag/AgCl). (B) Potential values from -300 to -800 mV (Ag/AgCl).

Table 1. List of the main Raman spectral bands of coumarin present in the Normal Raman spectrum of powder (Figure 13) and in the computed spectrum obtained by DFT/B3LYP with basis set: 6-311++g(d) (Figure 20). Computed Raman shifts have been rescaled according to the method described in [20]. Assignment to specific vibrational modes has been after [22], the page of the relevant references is quoted where relevant.

Experimental	Rescaled (DFT*0.98)	Symbol	Assignment	# Gaussian
450	441	α	ring stretching	6
733	725	β	ring stretching	13
766	755	γ	ring stretching	15
1030	1033	δ	semicircle stretching [22] p. 276	24
1125/1160	1122/1162	ϵ/η	CH scissoring	25/27
1180	1179	\omicron	CH scissoring	28
1235	1230	κ	CH wagging	29
1265	1263		CH scissoring	30
1284	1279	λ	CH bending [22] p. 277	31
1328	1350	μ	asym C=C stretching	32
1455	1460	ν	combination asym C=C stretching and CH wagging	34
1490	1496	ρ	combination asym C=C stretching and CH wagging [22] p. 267	35
1567	1575	σ	asym C=C stretching [22] p. 265	36
1606/1620	1622/1638	τ	asym C=C stretching [22] p. 265	37/38
1712	1764	-----	C=O stretching	39
2967/3060	3121, 3123, 3134, 3149, 3158, 3191	ξ_1/ξ_2	C-H stretching (aromatic)* [22] p. 388	40-41

3.3. Time-dependent *in situ* SERS during potentiostatic electrodeposition of Co

This type of experiments was carried out with the procedure described in the following. Prior to electrodeposition, the working electrode was polarised anodically at +800 mV for 45 min, in order to strip completely the Au substrate of electrodeposited Co. For details on the anodic behaviour of Co electrodes, see [26] and references therein contained. A cathodic potentiostatic step was subsequently applied and time-dependent Raman spectra were simultaneously recorded. The steps we considered were: -300 (Figure 6), -400 (Figure 7), -500 (Figure 8) and -600 mV (Figure 9). In general, at the onset

of Co deposition, the band assigned to $\nu(\text{CN})$ is observed and subsequently it tends to vanish as, for the reason mentioned above (Section 3.2).

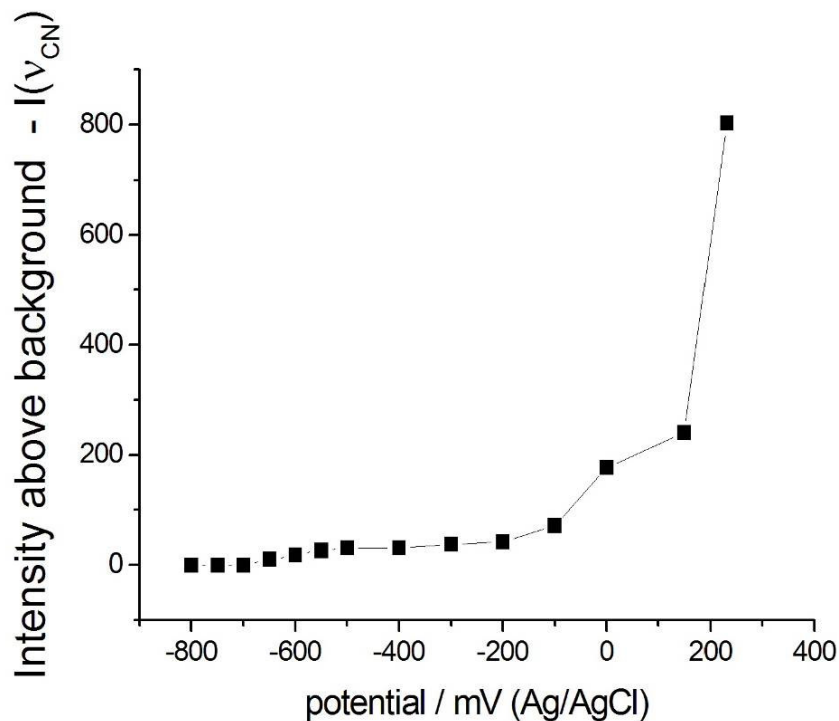


Figure 5. Intensity change of the $\nu(\text{CN})$ band with the applied cathodic potential (measurements corresponding to Figure 4).

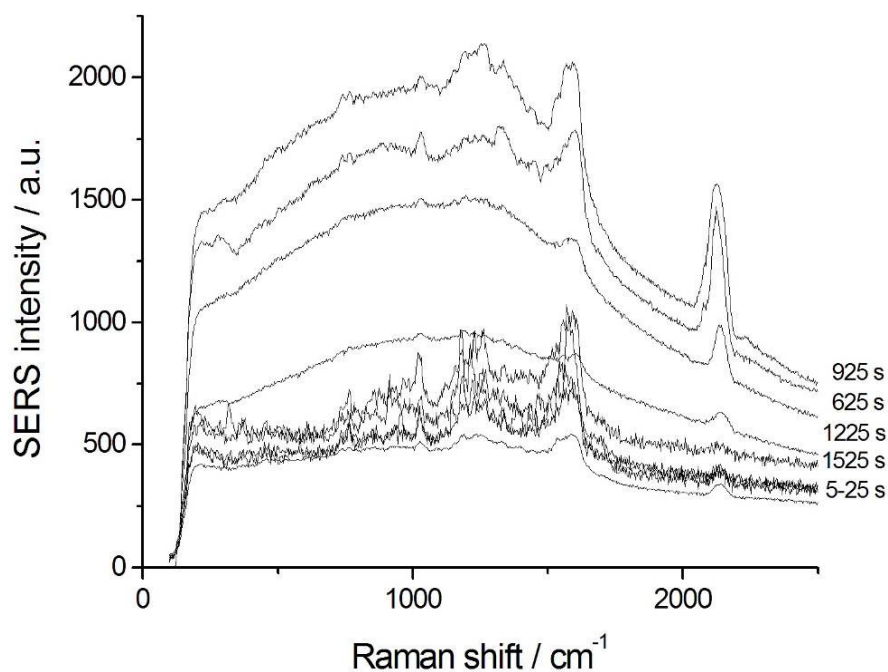


Figure 6. Time dependent SERS spectra measured during the electrodeposition of Co at -300 mV.

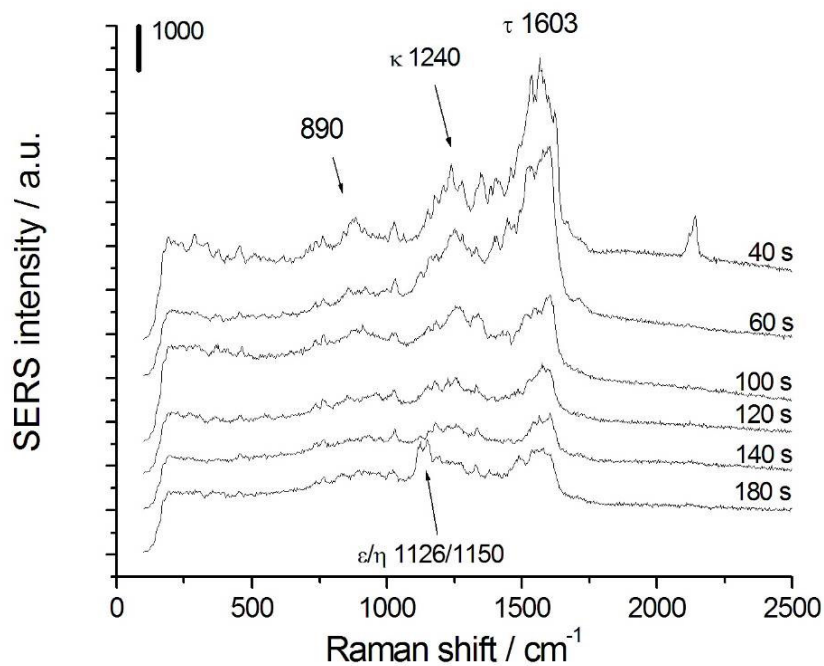
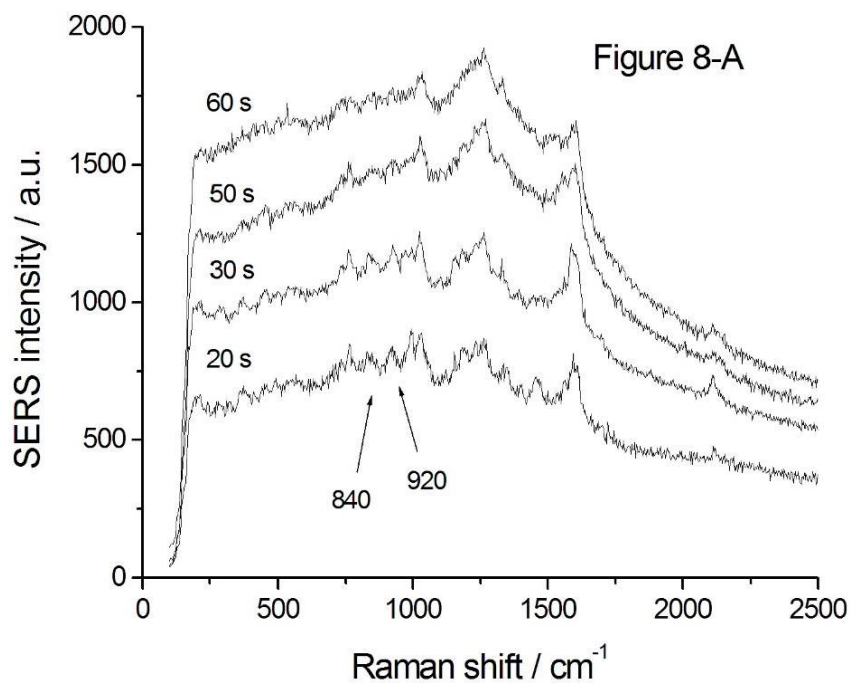


Figure 7. Time dependent SERS spectra measured during the electrodeposition of Co at -400 mV. (A): 20÷180 s, (B): 240÷440 s. The plots of Figure 7A have been spaced for clarity.



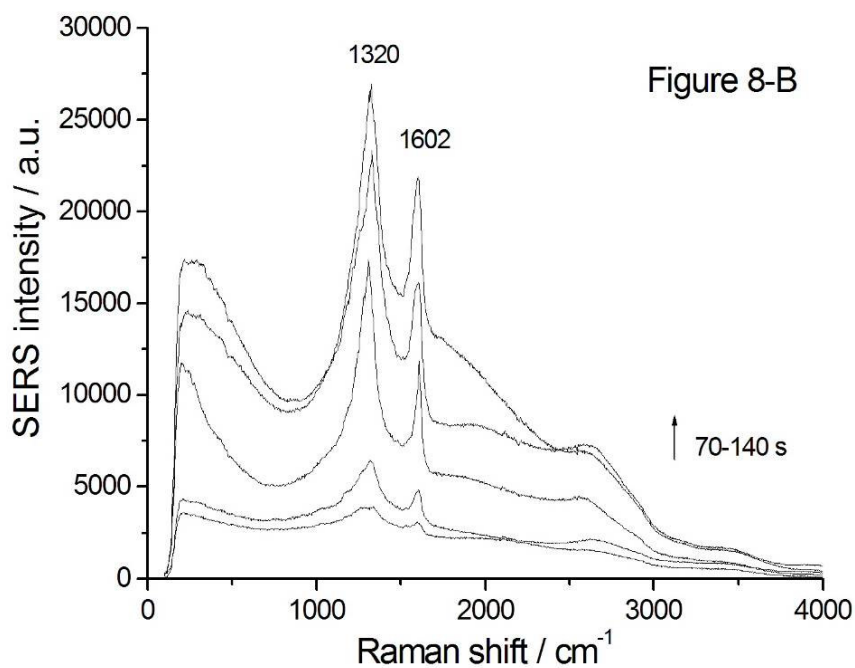
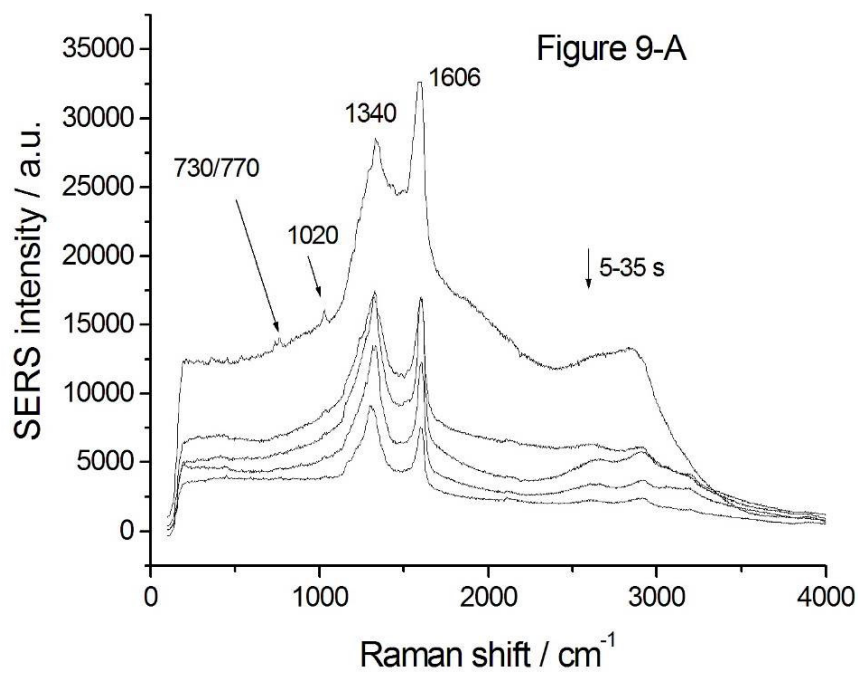


Figure 8. Time dependent SERS spectra measured during the electrodeposition of Co at -500 mV. (A): 20÷60 s, (B): 70÷140 s. The plots of Figure 8A have been spaced for clarity



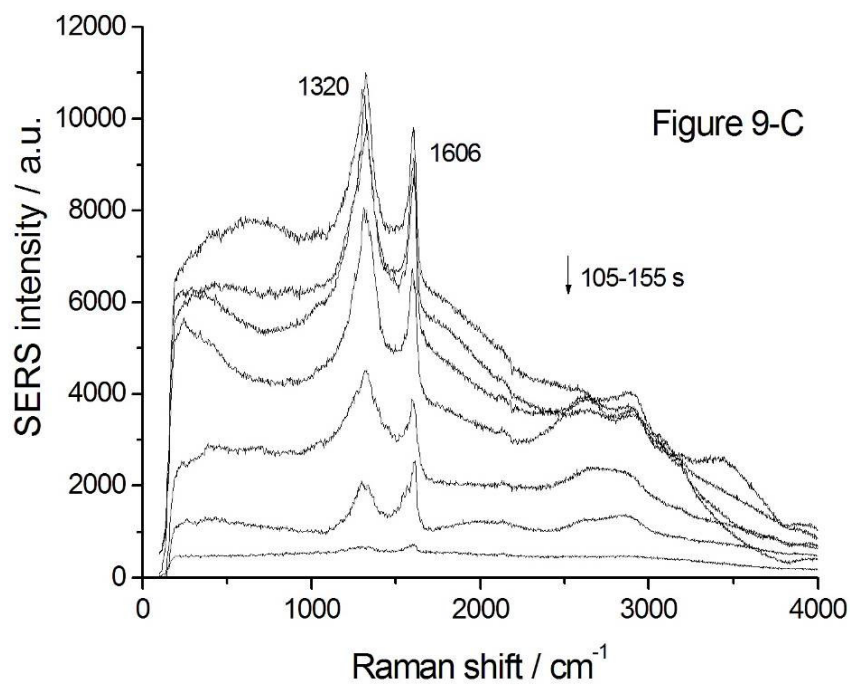
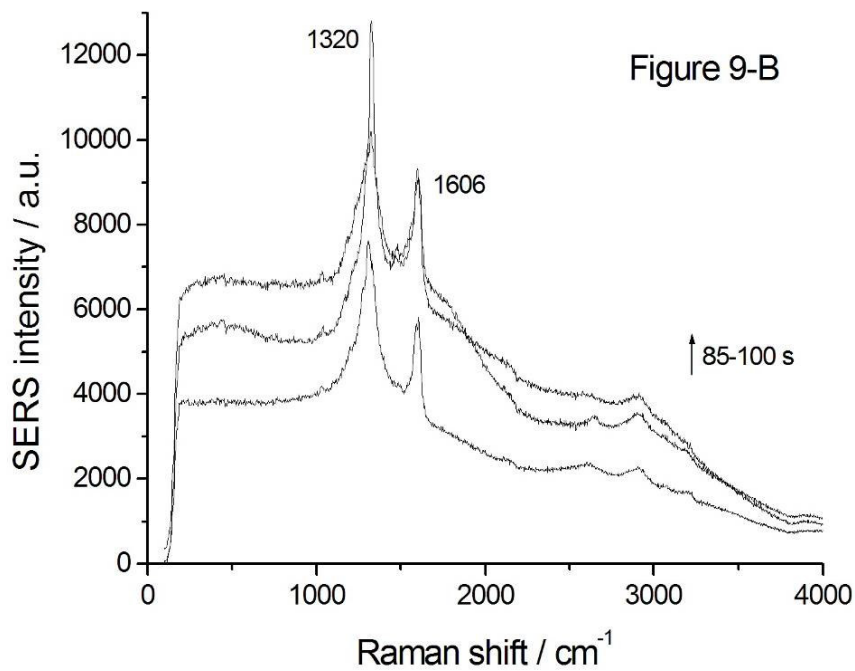


Figure 9. Time dependent SERS spectra measured during the electrodeposition of Co at -600 mV. (A): 5÷35 s; (B): 85÷100 s; (C) 105÷155 s.

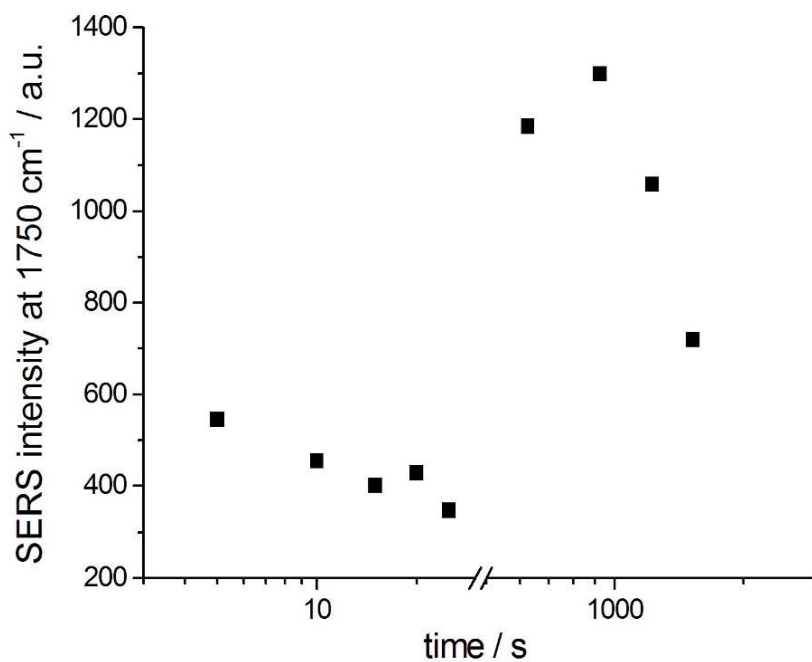


Figure 10. Variation of the SERS background intensity with Co electrodeposition time at -300 mV.

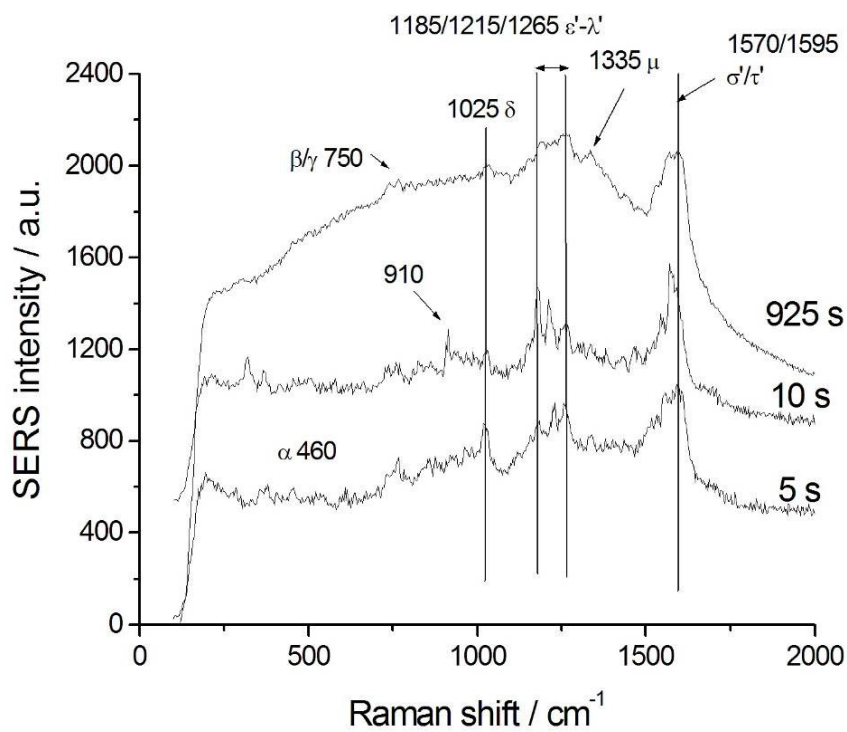


Figure 11. Chief changes in spectral pattern observed during the electrodeposition of Co at -300 mV at different times. Greek letters with apex denote bands whose positions are different from those of unreacted coumarin.

In Figure 6 we report the spectra measured at -300 mV. The electrochemical deposition generates SERS-active sites, whose activity increases after a few minutes of Co plating - as can be assessed from the variation of the $\nu(\text{CN})$ peak intensity -, possibly owing to the formation of discontinuous Co clusters on the Au surface of the cathode. At higher electrodeposition times, the signal decreases owing to the increase of the surface coverage with electrodeposited Co (Figure 10). As the deposition time increases, a wide fluorescence band was recorded.

As far as the spectral pattern is concerned, the following characteristics can be highlighted (Figure 11):

- i) bands β/γ , δ and μ are unchanged with respect to coumarin powder;
- ii) bands belonging to the groups $\epsilon-\lambda$ and σ/τ are modified, denoting reactivity of the organic additive.

Other minor variations of the spectral pattern can be also noticed. In particular, a peak at ca. 910 cm^{-1} was transiently (Figure 11, 10 s) observed, that can be assigned to the asymmetric stretching of condensed rings; the enhancement of this band may indicate a vertical orientation of the aromatic system.

Of course, on the basis of the available spectroscopic evidence, is not possible to draw a unique mechanistic conclusion; it is nevertheless possible to assert the presence of adsorbed reaction products formed under specific electrochemical conditions. In fact, by comparing the experimental and simulated spectra, the variation of spectral pattern can be explained with the formation of some reaction products of coumarin (Tables 1-4).

In particular:

- i) The new bands $\epsilon'-\lambda'$ found at 1185, 1215 and 1265 cm^{-1} can be tentatively assigned to the O-H scissoring, C-H wagging and Ph-OH stretching of hydrolyzed coumarin. In fact, the simulated spectrum of SH exhibits a triplet in the region of interest - related to these vibrations - while the remaining structures (S2÷S4) do not show any bands of appreciable intensity in this range (Figure 12).

- ii) The peaks σ/τ , well defined in the spectrum of solid coumarin (Figure 13), evolve to the more complicated structure σ'/τ' , that is a convolution of several bands, assigned to the asymmetric and symmetric stretching of aromatic C=C, combined with the stretching of aliphatic C=C in SH. In the same region, the simulated spectra of S2, S3 and S4 show only a very weak vibration at 1650 cm^{-1} that does not match the experimental data (Figure 12).

In Figure 7 we report the time-dependent spectra recorded at -400 mV. Also in this case we observed a progressive increase of the SERS activity with the deposition time; moreover, the SERS activity obtained at -400 mV is sensitively higher than the one obtained at -300 mV.

Table 2. List of the main Raman bands observed in the computed spectrum of hydrolysed coumarin (SH) obtained by DFT/B3LYP with basis set: 6-311++g(d) (Figure 12).

DFT	Rescaled (DFT*0.98)	Assignment	# Gaussian
785	769	Combination stretching	21
886/912	868/894	ring asym stretching combined with COH stretching	23/25
898	880	Out of plane	24
1071	1050	Semicircle stretching	29
1191/1193	1167/1170	C-H and O-H scissoring	31/32
1239	1214	C-H wagging	34
1286	1260	Ph-OH stretching	35
1294	1268	C-H wagging	36
1330	1303	C-O-H stretching	37
1337	1310	C-H wagging	38
1377	1349	OH bending in the group Ph-OH	39
1398	1370	C-H bending in the vinyl group	40
1624	1590	sym C=C stretching	43
1649	1616	asym C=C stretching	44
1681	1648	Vinyl C=C stretching	45

Table 3. Assignment of the Raman bands observed in the computed spectra of the structures S1, S2, S3, S4 and SH at ca. 1240 cm⁻¹. The spectra were obtained by DFT/B3LYP with basis set: 6-311++g(d) (Figure 12).

Structure	DFT	Rescaled (DFT*0.98)	Assignment	# Gaussian
S1	1255	1230	Wagging	29
	1286	1260		30
S2	1236	1210	Ph-OH bending	36
	1278	1250	C-OH bending	37
S3	1245	1220	aliphatic C-H torsion	36
	1273	1247	Ph-OH stretching	37
S4	1257	1232	aliphatic C-H torsion	33
	1276	1250	Ph-OH stretching	34
SH	1287	1261	Ph-OH stretching	35
	1294	1268	Vinyl =C-H bending	36

Table 4. Assignment of the Raman bands observed in the theoretical spectra of the structures S1, S2, S3, S4 and SH at ca. 1335 cm⁻¹. The spectra were obtained by obtained by DFT/B3LYP with basis set: 6-311++g(d) (Figure 12).

Structure	DFT	Rescaled (DFT*0.98)	Assignment	# Gaussian
S1	1376	1348	Asymmetric stretching	32
S2	1360	1333	C-H torsion	42
	1373	1345		
S3	1355	1328	C-H torsion	40
	1372	1344	Aromatic CH scissoring	41
S4	1357	1330	C-H torsion	37
	1372	1344	Aromatic CH scissoring	38
SH	1377	1350	O-H bending combined with aromatic C-H scissoring	39

Table 5. Assignment of the Raman bands observed in the theoretical spectra of the structures S1, S2, S3, S4 and SH in the range of 1600-1700 cm⁻¹. The spectra were obtained by obtained by DFT/B3LYP with basis set: 6-311++g(d) (Figure 12).

Structure	DFT	Rescaled (DFT*0.98)	Assignment	# Gaussian
S1	1607	1575	condensed ring stretching	36
	1657	1624	condensed ring stretching	37
	1673	1640	condensed ring stretching	38
S2	1640	1607	Asym aromatic stretching	48
	1660	1627	Sym aromatic stretchin	49
S3	1635	1620	Asym aromatic stretching	50
	1654	1621	Sym aromatic stretching	51
S4	1653	1620	aromatic stretching	48
SH	1624	1591	aromatic stretching	43
	1650	1617	aromatic stretching	44
	1680	1646	aliphatic C=C stretching	45

As the deposition time increases, we observed small changes in the spectral pattern, probably related to some different orientation of adsorbates or to 3D electrocrystallization: both factors can in fact result in the same type of spectral variations (for a discussion of this point, see, e.g. [27]). The most important changes are related to the peaks at ca. 1350 (μ -type) and ca. 1603 (τ -type) cm⁻¹ and to the formation of a fluorescence band.

In particular, we can observe that:

i) A few minutes after the beginning of electrodeposition, a new band is formed at ca. 890 cm⁻¹ and the relative intensity of the peak at ca. 1240 cm⁻¹ (κ -type) increases versus the ϵ/η -type bands at 1126/1150 cm⁻¹;

ii) for deposition time longer than 5 minutes, the two peaks at 1335 cm^{-1} (μ -type), and 1603 cm^{-1} (τ -type) become the predominant bands in the spectra. Moreover, the strong fluorescence band indicates some reactivity of the coumarin.

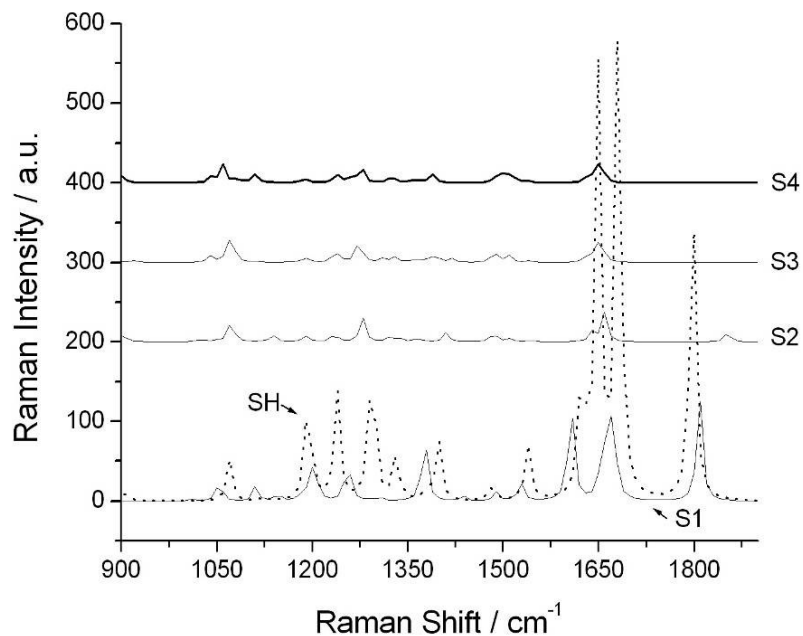


Figure 12. Raman spectra of the following structures: coumarin (S1), 3(2-hydroxy phenyl propionic acid) (S2), o-hydroxy phenyl propanol (S3), n-propyl phenol (S4), (o-hydroxy cinnamic acid) (SH), simulated as DFT- B3LYP/6-31+g(d).

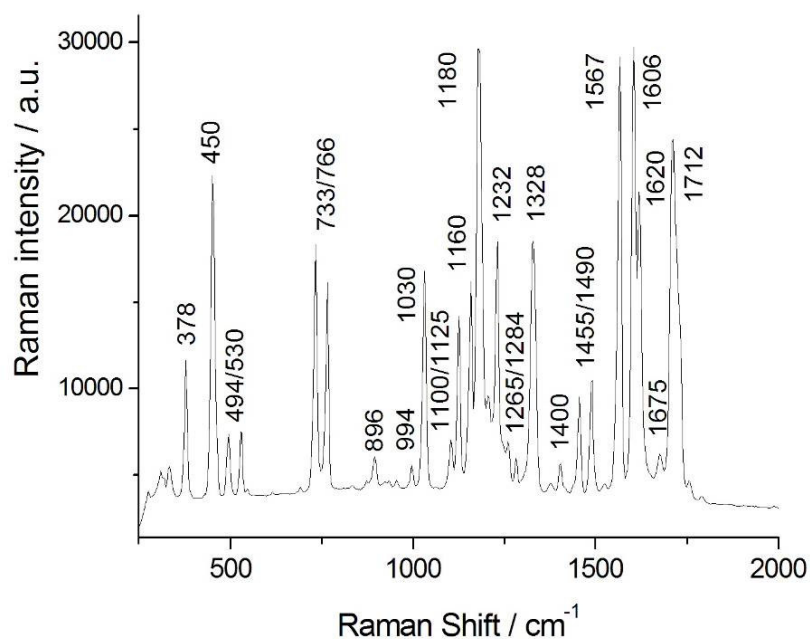


Figure 13. Normal Raman spectrum of coumarin powder.

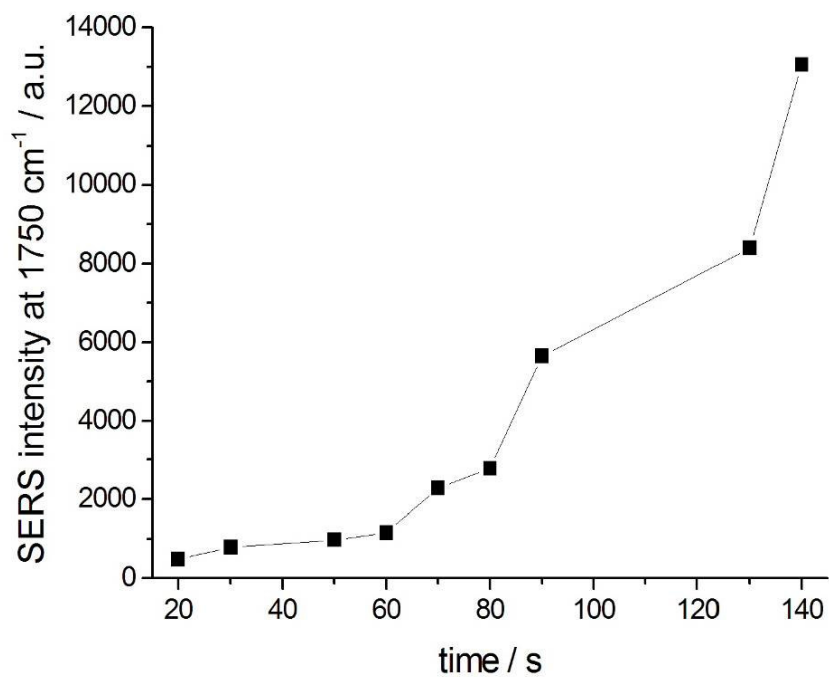


Figure 14. Time-dependence of the SERS background intensity recorded during Co electrodeposition at -500 mV.

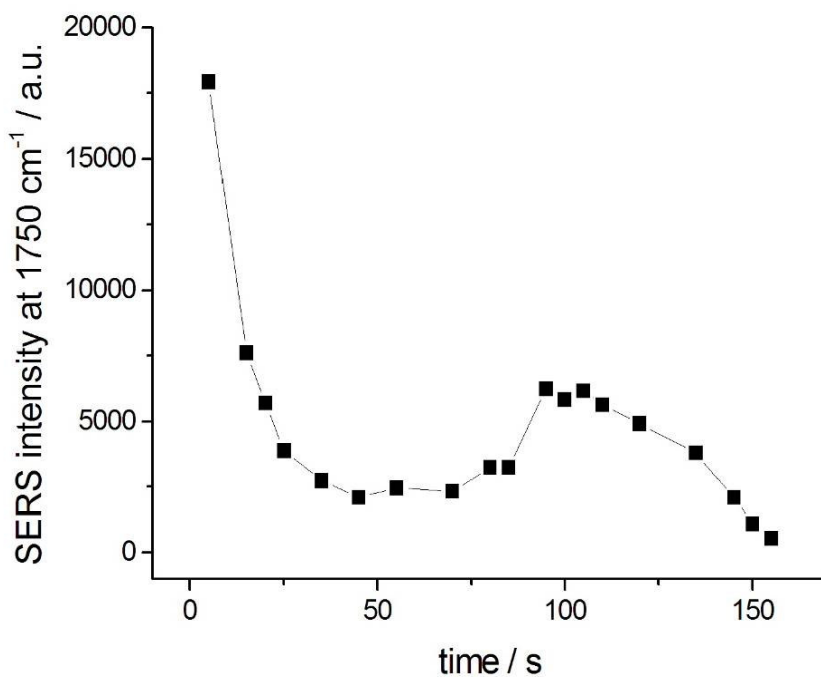


Figure 15. Time-dependence of the SERS background intensity recorded during Co electrodeposition at -600 mV.

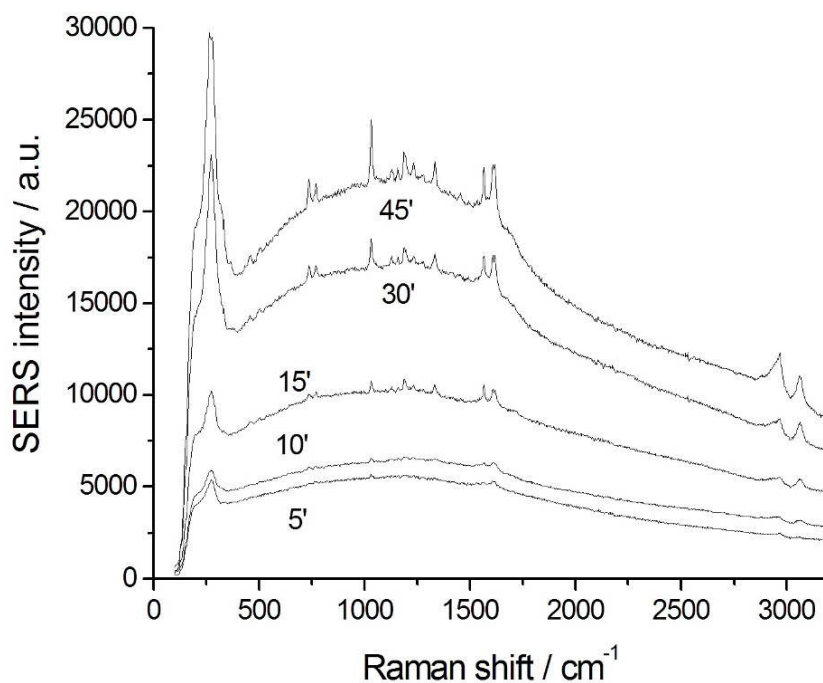


Figure 16. Time dependent SERS spectra measured during the stripping at +800 mV of a Co layer pre-electrodeposited at -300 mV.

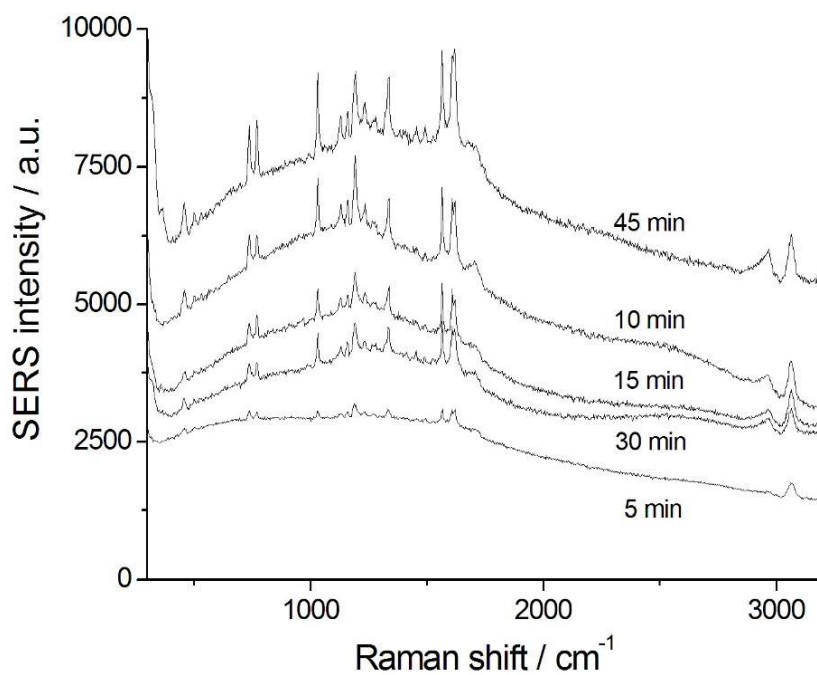


Figure 17. Time dependent SERS spectra measured during the stripping at +800 mV of a Co layer pre-electrodeposited at -400 mV.

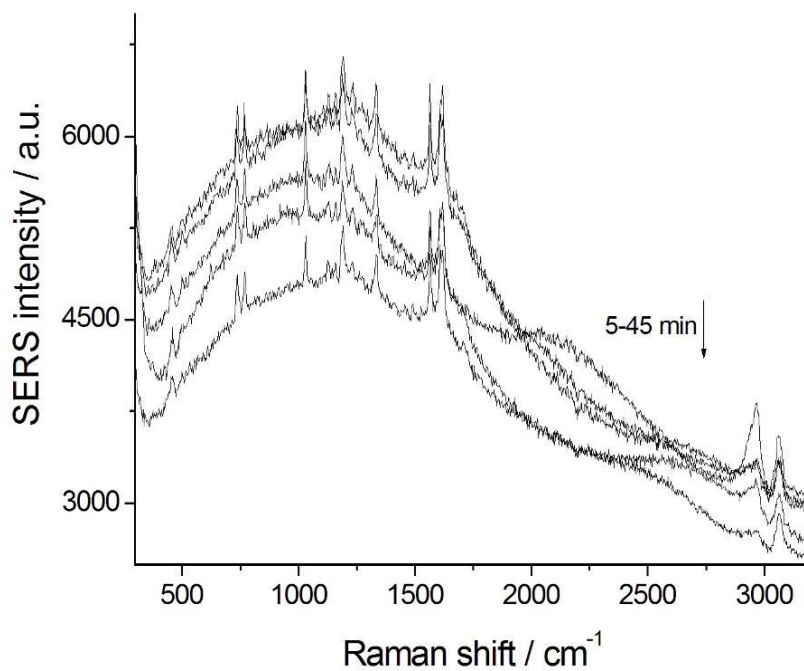


Figure 18. Time dependent SERS spectra measured during the stripping at +800 mV of a Co layer pre-electrodeposited at -500 mV.

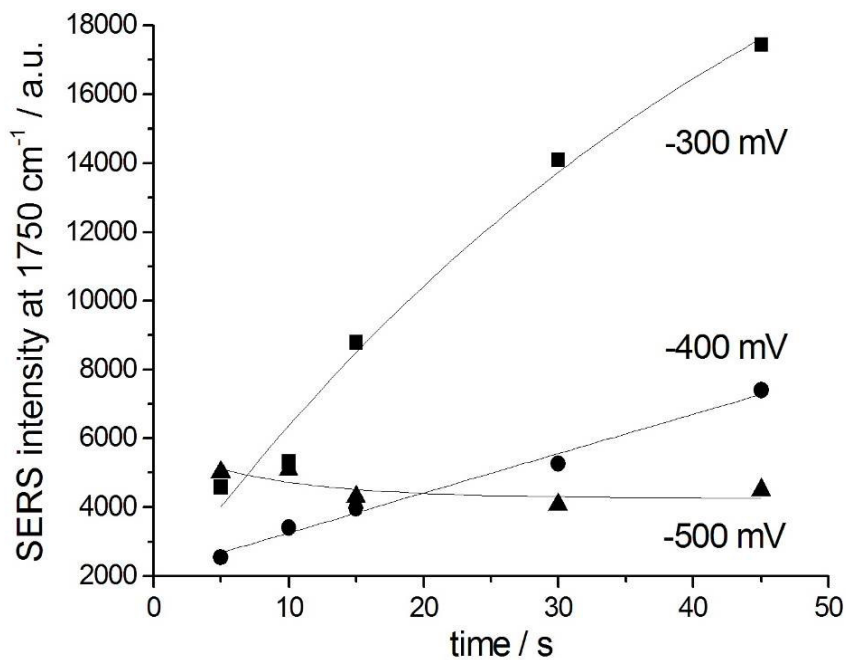


Figure 19. Time-dependence of the SERS background intensity recorded during the stripping at +800 mV of Co films electrodeposited the indicated potentials.

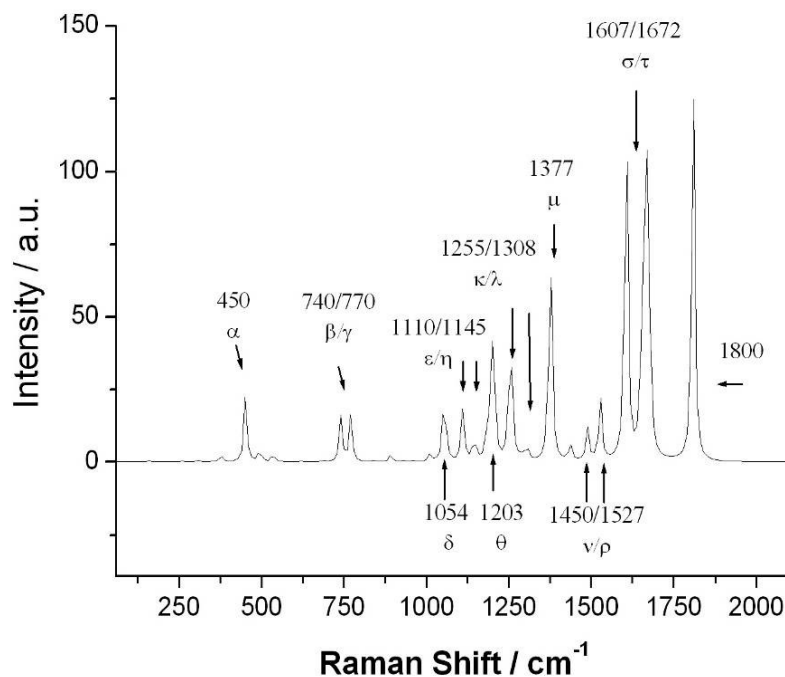


Figure 20. Computed Raman spectrum of coumarin (DFT- B3LYP/6-31+g(d)).

As far as the assignment of the κ -type band is concerned, all the simulated structures exhibit weak vibrations around 1240 cm^{-1} (see Table 3). On the basis of computed spectra, in particular taking into account the intensity and the shape of the peaks, the best assignment of this band is a combination of Ph-OH stretching and vinyl CH bending of SH.

As far as the type- μ bands are concerned, a weak peak at ca. 1335 cm^{-1} is present in the reduction products S2, S3 and S4, that can be assigned to CH torsion. In the SH hydrolyzed structure, a combination band of OH bending e CH scissoring was computed at 1350 cm^{-1} .

Similarly, the triplet centred 1603 cm^{-1} can be assigned to the symmetric and asymmetric stretching of aromatic ring of different reaction products (see Table 5 and Figure 12).

In Figure 8 we report the SERS measurements carried out during the electrodeposition of Co at -500 mV . The SERS activity increases with the deposition time and increases to valued higher then those found at lower cathodic potentials (Figure 14). Since relatively short deposition times, the spectral pattern reveals some changes with respect to that of unreacted coumarin. The new, weak peaks found at 840 and 920 cm^{-1} can be assigned to the wagging of aromatic CH. Other small spectral alterations, combined with the formation of a fluorescence band, were detected at longer deposition time, in analogy to the phenomenology highlights at lower cathodic potentials and discussed above. Some details on the electrochemistry of related organics can be found in [28].

In Figure 9 we show the SERS measurements carried out during the electrodeposition of Co at -600 mV . Again, we can highlight the predominance of the two peaks at 1340 cm^{-1} and 1606 cm^{-1} , and the formation of a fluorescence band. Moreover, some peaks belonging to the unreacted coumarin can

be found: β/γ ($730/770\text{ cm}^{-1}$) e δ (1020 cm^{-1}). Is it also noteworthy that the SERS-activity achieved during these measurements is considerably high even at low deposition time (Figure 15).

3.4. Time-dependent *in situ* SERS during the potentiostatic stripping of Co.

In order to test the evolution of the interfacial chemistry during anodic polarisation - in view of the use of soluble anodes in industrial plating processes - as well as to assess the SERS activity related to the formation of dissolution morphologies, we carried out spectroelectrochemical measurements in the Co bath during the stripping at 800 mV of Co layers pre-electrodeposited at -300, -400 e -500 mV; the corresponding spectra are shown in Figures 16, 17 and 18, respectively.

All the measurements exhibit a very high stability of the spectral pattern and a variation of the SERS signal with the time. The SERS intensity tends to increase in the case of Co layers grown at -300 and -400 mV, but it decreases during the stripping of Co films formed at -500 mV (Figure 19). This kind of time-dependence is related to the stripping of Co clusters, that results in the formation of SERS-active surfaces, probably both in terms of morphology (roughness) and composition (discontinuity of the Co layer). As proved in [25, 29], SERS spectroscopy carried out during anodic dissolution can also provide useful information about the composition of thick electrodeposited coatings. The surfaces obtained after complete stripping (+800 mV, 45 minutes) of the Co coating have been used for the OCP investigations at the Au surface described in Section 3.1.

4. CONCLUSIONS

In this research, we carried out SERS measurements during the electrodeposition and anodic dissolution of Co films from a coumarin-containing bath. The following types of electrochemical polarisation procedures were considered: (i) cathodic potential staircase; (ii) potentiostatic electrodeposition; (iii) potentiostatic stripping of potentiostatically pre-electrodeposited Co layers.

Notwithstanding the limited SERS enhancement, we could measure potential-dependent spectra that allowed the identification of bands that allowed spectral assignment of coumarin and its reduction and hydrolysis products. Furthermore, the degree of surface enhancement typically tends to increase with electrodeposition time and we observed spectral patterns dependent on electrodeposition potential and time as well as development of wide fluorescence bands, denoting interfacial reactivity of the organic and morphological evolution of the growing surface (see, e.g., [30]). Stripping measurements have shown a very high spectral quality and a remarkable sensitivity to the mode of grown of Co film.

The measurements presented in this work extend the *in situ* SERS technique - widely demonstrated for the electrodeposition of SERS-active metals (see, e.g., [31]) - to the metals belonging to the Fe group, that present a great interest for applications.

References

1. O.E. Kongstein, Æ.G.M. Haarberg, Æ.J. Thonstad, *J. Appl. Electrochem*, 37 (2007) 669.
2. J.P. Celis, P. Cavallotti, J. Machado Da Silva and A. Zielonka, *Trans. Inst. Met. Finish.*, 76 (1998) 163.
3. S. Franz, P.L. Cavallotti, M. Bestetti, V. Sirtori, L. Lombardi, *J. Magn. Magn. Mat*, 272–276 (2004) 2430.
4. D. Grujicic, B. Pesic, *J. Magn. Magn. Mat*, 285 (2005) 303.
5. N.B. Chaure, P. Stamenov, F.M.F. Rhen, J.M.D. Coey, *J. Magn. Magn. Mat*, 290–291 (2005) 1210.
6. B.O'Brien, K.J. Stebe, P.C. Searson, *J. Phys. Chem. C*, 111 (2007) 8686.
7. A. Vicenzo, P.L. Cavallotti, *Electrochim. Acta*, 49 (2004) 4079.
8. V.M. Kozlov, L. Peraldo Bicelli, in: H.S. Nalwa (Ed.), *Handbook of Thin Film Materials*, vol. 1, Academic Press, San Diego Cal., 2002, pp. 559-586.
9. L. Liao, W. Liu, X. Xiao, *J. Electroanal. Chem.*, 566 (2004) 341.
10. N.D. Nikolic, H. Wang, H. Cheng, C.A. Guerrero, N. Garcia, *J. Magn. Magn. Mat.*, 272-276 (2004) 2436.
11. M. Mouanga, L. Ricq, G. Douglade, P. Berçot, *Surf. Coat. Technol.*, 201 (2006) 762.
12. K.R. Marikkannu, G. Paruthimal Kalaigan, T. Vsudevan, *J. Alloys and Compounds*, 438 (2007) 332.
13. M. Mouanga, L. Ricq, L. Ismaili, B. Refouvet, P. Berçot, *Surf. Coat. Technol.*, 201 (2007) 7143.
14. Z.-Q. Tian, B. Ren, in: P.R. Unwin (Ed.), *Encyclopedia of Electrochemistry*, vol. 3, Wiley-VCH Darmstadt (D), 2003, pp. 572-659.
15. B. Ren, G.-K. Liu, X.-B. Lian, Zh.-L. Yang, Z.-Q. Tian, *Anal. Bioanal. Chem.*, 388 (2007) 29.
16. Y. Xie, D.Y. Wu, G.K. Liu, Z.F. Huang, B. Ren, J.W. Yan, Z.L. Yang, Z.Q. Tian, *J. Electroanal. Chem.*, 554-555 (2003) 417.
17. J.-L. Yao, J. Tang, D.-Y. Wu, D.-M. Sun, K.-H. Xue, B. Ren, B.-W. Mao, Z.-Q. Tian, *Surf. Sci.*, 514 (2002) 108.
18. Q.-J. Huang, X.-Q. Li, J.-L. Yao, B. Ren, W.-B. Cai, J.-S. Gao, B.-W. Mao, Z.-Q. Tian, *Surf. Sci.*, 427-428 (1999) 162.
19. Frisch, M. J.; Trucks, G. W.; Schlegel, H. B.; Scuseria, G. E.; Robb, M. A.; Cheeseman, J. R.; Montgomery, J. A., Jr.; Vreven, T.; Kudin, K. N.; Burant, J. C.; Millam, J. M.; Iyengar, S. S.; Tomasi, J.; Barone, V.; Mennucci, B.; Cossi, M.; Scalmani, G.; Rega, N.; Petersson, G. A.; Nakatsuji, H.; Hada, M.; Ehara, M.; Toyota, K.; Fukuda, R.; Hasegawa, J.; Ishida, M.; Nakajima, T.; Honda, Y.; Kitao, O.; Nakai, H.; Klene, M.; Li, X.; Knox, J. E.; Hratchian, H. P.; Cross, J. B.; Bakken, V.; Adamo, C.; Jaramillo, J.; Gomperts, R.; Stratmann, R. E.; Yazyev, O.; Austin, A. J.; Cammi, R.; Pomelli, C.; Ochterski, J. W.; Ayala, P. Y.; Morokuma, K.; Voth, G. A.; Salvador, P.; Dannenberg, J. J.; Zakrzewski, V. G.; Dapprich, S.; Daniels, A. D.; Strain, M. C.; Farkas, O.; Malick, D. K.; Rabuck, A. D.; Raghavachari, K.; Foresman, J. B.; Ortiz, J. V.; Cui, Q.; Baboul, A. G.; Clifford, S.; Cioslowski, J.; Stefanov, B. B.; Liu, G.; Liashenko, A.; Piskorz, P.; Komaromi, I.; Martin, R. L.; Fox, D. J.; Keith, T.; Al-Laham, M. A.; Peng, C. Y.; Nanayakkara, A.; Challacombe, M.; Gill, P. M. W.; Johnson, B.; Chen, W.; Wong, M. W.; Gonzalez, C.; Pople, J. A. *Gaussian 03*; Gaussian, Inc.: Pittsburgh, PA, 2003.
20. J.B. Foresman, Æ. Frisch, *Exploring Chemistry with Electronic Structure Methods*; Gaussian Inc.: Pittsburgh, 1996, pp 64 and 90.
21. *Aldrich Handbook of FT-IR Spectra Vol.2*, p. 322B, C8560-2.
22. N.B. Colthup, L.H. Daly, S.E. Wiberley, *Introduction to Infrared and Raman Spectroscopy*, Academic Press (Boston), 1990.
23. M. Fleischmann, Z.Q. Tian, L.J. Li, *J. Electroanal. Chem.*, 217 (1987) 397.
24. L.W.H. Leung, M.J. Weaver, *J. Electroanal. Chem.*, 217 (1987) 367.

25. B. Bozzini, A. Fanigliulo, *Trans. Inst. Met. Finish.*, 80 (2002) 25.
26. M.E.G. Lyons, M.P. Brandon, *Int. J. Electrochem. Sci.*, 3 (2008)1425.
27. B. Bozzini, P.L. Cavallotti, A. Fanigliulo, G. Giovannelli, C. Mele, S. Natali, *J. Solid State Electrochem.*, 8 (2004) 147.
28. S. Riahi, M.R. Ganjali, H. Khajehsharifi, P. Norouzi, S. Taghipoor, *Int. J. Electrochem. Sci.*, 4 (2009) 122.
29. B. Bozzini, L. D'Urzo, G. Giovannelli, C. Mele, *Trans. Inst. Met. Finish.*, 82 (2004) 118.
30. B. Bozzini, L. D'Urzo, C. Mele, *J. Electrochem. Soc.*, 152 (2005) C255.
31. B. Bozzini, *Recent Research Developments in Electrochemistry*, 8 (2005) 25.